Mathematical Problems in Engineering, 2002, Vol. 8(4–5), pp. 451–473

Sliding Mode Control on Electro-Mechanical Systems

VADIM I. UTKIN[a,*] and HAO-CHI CHANG[b,†]

[a]*Departments of Electrical and Mechanical Engineering,* [b]*Department of Mechanical Engineering, The Ohio State University, Columbus, OH 43210, USA*

(Received 13 May 2002)

The first sliding mode control application may be found in the papers back in the 1930s in Russia. With its versatile yet simple design procedure the methodology is proven to be one of the most powerful solutions for many practical control designs. For the sake of demonstration this paper is oriented towards application aspects of sliding mode control methodology. First the design approach based on the regularization is generalized for mechanical systems. It is shown that stability of zero dynamics should be taken into account when the regular form consists of blocks of second-order equations. Majority of applications in the paper are related to control and estimation methods of automotive industry. New theoretical methods are developed in the context of these studies: sliding made nonlinear observers, observers with binary measurements, parameter estimation in systems with sliding mode control.

Key words: Sliding mode control; Inverted pendulum; Induction motor; Binary sensor; VGT; EGR; Diesel engines; Alternator; Air conditioner; Climate control; ABS; Optimization

1 INSTEAD OF INTRODUCTION

One of the authors was appointed as a Professor at the Ohio State University in 1994 – the position established by Ford Motor Company and has been working on applications of the sliding mode control methodology for automotive industry.

The paper is some kind of report about the results of these studies. The basic concepts of control and estimation methods in the framework of Sliding Mode Control Theory behind the research were originated at the Institute of Control Sciences, where the author was privileged to work and had the unique opportunity to contact outstanding scientists. Creative atmosphere for the research along with democratic spirit of scientific discussions were decisive factors for the further professional career of the author.

The paper embraces wide range of automotive applications (automotive alternator, diesel and combustion engines, ABS system, climate control), which needed further development of the well-known methods. These studies have been performed in long-term cooperation with the second author (Ph.D. student of the Ohio State University).

2 SLIDING MODE FOR MECHANICAL SYSTEMS

Although the design of the sliding mode control for nonlinear multivariable systems has been extensively studied in many books and papers, the design procedures for such high order

* Corresponding author. E-mail: utkin@ee.eng.ohio-state.edu
† E-mail: chang@rcltel.eng.ohio-state.edu

ISSN 1024-123X print; ISSN 1563-5147 online

nonlinear control systems may be complicated and vary from case to case. The objective of this section is to develop design methods for the nonlinear mechanical systems governed by a set of nonlinear interconnected second-order equations which are common for mechanical systems. The proposed approach assumes that control systems can be transformed into a regular form [3], which facilitates the controller design. Consider a general mechanical system, $J(q)\ddot{q} = f(q, \dot{q}) + Bu$, where $q \in \Re^n$ and $u \in \Re^m$, is a vector of control forces, $\operatorname{rank} B = m$. The inertia matrix $J(q)$ in mechanical systems is nonsingular and positive definite, B is a full rank matrix. Hence $J^{-1}(q)B$ is a full rank matrix as well. The components of vector q may be reordered such that in the motion equation

$$\begin{aligned} \ddot{q}_1 &= \tilde{f}_1(q, \dot{q}) + \tilde{B}_1(q)u \\ \ddot{q}_2 &= \tilde{f}_2(q, \dot{q}) + \tilde{B}_2(q)u, \\ q &= \begin{bmatrix} q_1 \\ q_2 \end{bmatrix}, \quad q_1 \in \Re^{n-m}, \quad q_2 \in \Re^m, \qquad \begin{bmatrix} \tilde{f}_1 \\ \tilde{f}_2 \end{bmatrix} = J^{-1}f, \\ \begin{bmatrix} \tilde{B}_1 \\ \tilde{B}_2 \end{bmatrix} &= J^{-1}B, \quad \det(\tilde{B}_2) \neq 0, \end{aligned} \tag{2.1}$$

According to the regular form technique [3] the coordinate transformation $z = \phi(q) \in \Re^{n-m}, y = q_2$ with continuously differentiable function $\phi(q)$ should be found such that the mechanical system equation is reduced to the regular form consisting of a set of second order equations

$$\begin{aligned} \ddot{z} &= f_1(z, y, \dot{z}, \dot{y}) \\ \ddot{y} &= f_2(z, y, \dot{z}, \dot{y}) + B_2(z, y)u, \end{aligned} \tag{2.2}$$

where $\det(B_2) \neq 0$. In our case the top block equation in (2.2) depends on both vectors y and $\dot{y}$. This fact introduces some peculiarities which should be taken into account when designing sliding mode control. Further a stabilization task for different types of mechanical systems will be studied. It is assumed that the origin in a system state space is an equilibrium point of an open loop system, *i.e.*, $f_1(0, 0, 0, 0) = 0$ and $f_2(0, 0, 0, 0) = 0$. Based on this form two design approaches are demonstrated below:

First, the stability of the system zero dynamics with vector y as an output is checked. They are governed by the first equation (2.2) $\ddot{z} = f_1(z, 0, \dot{z}, 0)$ with $y = 0$ and $\dot{y} = 0$. If they are stable then sliding mode may be enforced in the manifold $s = \dot{y} + cy = 0$, $s \in R^m$ with scalar parameter $c > 0$, since $\operatorname{rank}(B_2) = m$. After sliding mode starts in $s = 0$ the state y tends to zero as a solution to $\dot{y} + cy = 0$, and then z decays as well because $\ddot{z} = f_1(z, 0, \dot{z}, 0)$ is stable.

Second, stability of the system zero dynamics with vector z as an output is checked. If $z(t) = 0$ then the zero dynamics equation are obtained from $f_1(0, y, 0, \dot{y}) = 0$. Note that the zero dynamics system is a set of first order equations while it was is a set of second order equations in the first approach. If the zero dynamics are stable then sliding mode is enforced in the manifold $s = f_1 + c_1 z + c_2 \dot{z} = 0$, the top equation of (2.2) becomes $\ddot{z} = -c_1 z - c_2 \dot{z}$ whose rate of decay may be selected by c_1 and c_2.

Third, assume that the function $f_1(z, y, \dot{z})$ does not depend on $\dot{y}$. Basically if $s = f_1 + c_1 z + c_2 \dot{z} = 0$, then $\ddot{z} = -c_1 z - c_2 \dot{z}$ holds and, as a result, $f_1(0, y, 0) = 0$ after $z(t) = 0$. Based on the assumption, $f_1(0, 0, 0, 0) = 0$ and $f_2(0, 0, 0, 0) = 0$, we may conclude

$f_1(0, 0, 0) = 0$, which means that y tends to zero as well. To provide the desired relationship $s = f_1 + c_1 z + c_2 \dot{z} = 0$ the following switching manifold is selected as

$$S = \dot{s} + \alpha s \tag{2.3}$$

where $s = f_1 + c_1 z + c_2 \dot{z}$ and $\alpha > 0$. As a result, the derivative of (2.3) depends on discontinuous control u which is necessary to enforce sliding mode. If Zero Dynamics are unstable then, following the methodology of the Regular Form approach, the state of the second block is handled as the control of the first one to stabilize the Zero Dynamics. Next sliding mode is enforced to provide the desired dependences between state variables (see [4] for more details about the design strategy for this design scenario).

For the sake of briefness, the following two applications demonstrate only the model and simulation/experiment results. Readers may refer to [4] for further details. First of all, the double inverted pendulum (Fig. 2.1(a)) is considered.

$$H\begin{bmatrix} \ddot{\theta}_1 \\ \ddot{\theta}_2 \end{bmatrix} + P\begin{bmatrix} \dot{\theta}_1 \\ \dot{\theta}_2 \end{bmatrix} + W = \begin{bmatrix} F_1 \\ F_2 \end{bmatrix}, \tag{2.4}$$

where

$$H = \begin{bmatrix} J_0 + I_1 + m_1 l_1^2 + m_2 L_1^2 & m_2 L_1 l_2 \cos(\theta_1 - \theta_2) \\ m_2 L_1 l_2 \cos(\theta_1 - \theta_2) & m_2 l_2^2 + I_2 \end{bmatrix},$$

$$W = \begin{bmatrix} -g(m_1 l_1 + m_2 L_1)\sin\theta_1 \\ -m_2 g l_2 \sin\theta_2 \end{bmatrix},$$

$$P = \begin{bmatrix} 0 & V\dot{\theta}_2 \\ -V\dot{\theta}_1 & 0 \end{bmatrix} \quad \text{and} \quad V = m_2 L_1 l_2 \sin(\theta_1 - \theta_2).$$

Each link of the pendulum is composed of mass m and inertia I. Total length of each link is L_i and the distance to center of gravity of each link from its pivot is l_i $(i = 1, 2)$. θ refers to the rotational angle from the vertical axis. It is assumed that only one control force, the motor torque $F_1 = u$, is available and F_2 is regarded as the disturbance torque to the pendulum.

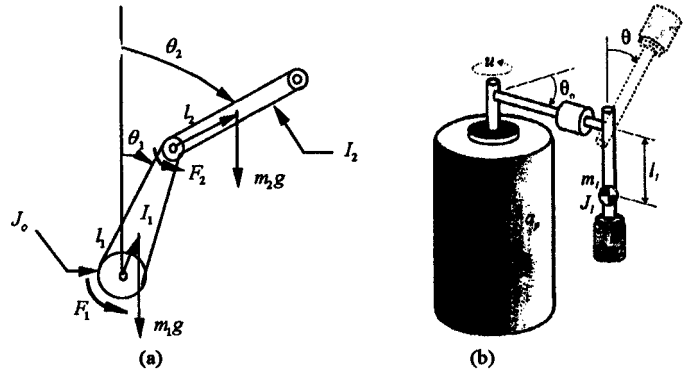

FIGURE 2.1 (a) Double inverted pendulum (b) Rotational inverted pendulum.

The control objective is to drive the mechanical system from a perturbed state to the desired equilibrium point $\theta_1 = \theta_2 = 0$.

Numerical simulation is performed to verify proposed control algorithm. Evidently observed from the following Figure 2.2, sliding mode control algorithm is able to keep the double pendulum upright.

The second interesting application is rotational inverted pendulum (Fig. 2.1(b)). Its governing equations are summarized below:

$$\begin{cases} \ddot{\theta}_0 = -a_p \dot{\theta}_0 + K_p u \\ \ddot{\theta}_1 = -\dfrac{C_1}{J_1}\dot{\theta}_1 + \dfrac{m_1 g l_1}{J_1}\sin\theta_1 + \dfrac{K_1}{J_1}\ddot{\theta}_0, \end{cases} \tag{2.5}$$

where m_1 and J_1 are mass and inertia of the pendulum, l_1 is the distance from the center of gravity of the link to its pivot point, g is the gravity acceleration, and C_1 is the frictional constant between the pendulum and the rotating base. The coordinate θ_0 represents the rotational angle of the base with respect to some horizontal axis (usually defined as the starting position) and θ_1 is the rotational angle of the pendulum with respect to the vertical axis. $\theta_0 = 0$ refers to the unstable equilibrium point. SMC control is designed such that both Inverted Pendulum and the Base angles are stabilized simultaneously. Even more additional sloshing water and metal bolts are attached at the end of pendulum for the purpose of demonstrating algorithm robustness. Satisfactory results may be found in the following Figure 2.3 which demonstrates the effectiveness and robustness of the controller.

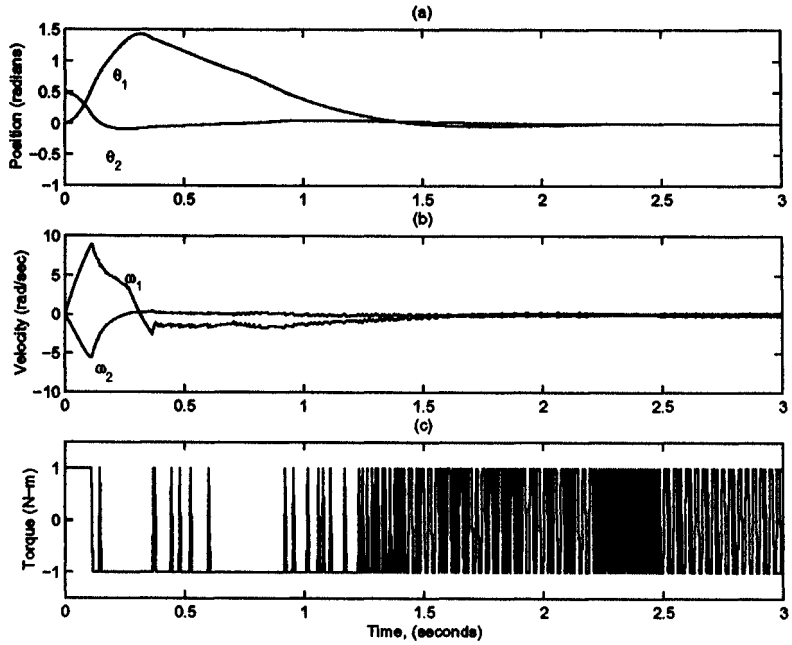

FIGURE 2.2 Double inverted pendulum simulation results using SMC with maximum initial deviation $\theta_2(0) = 0.49$ rad.

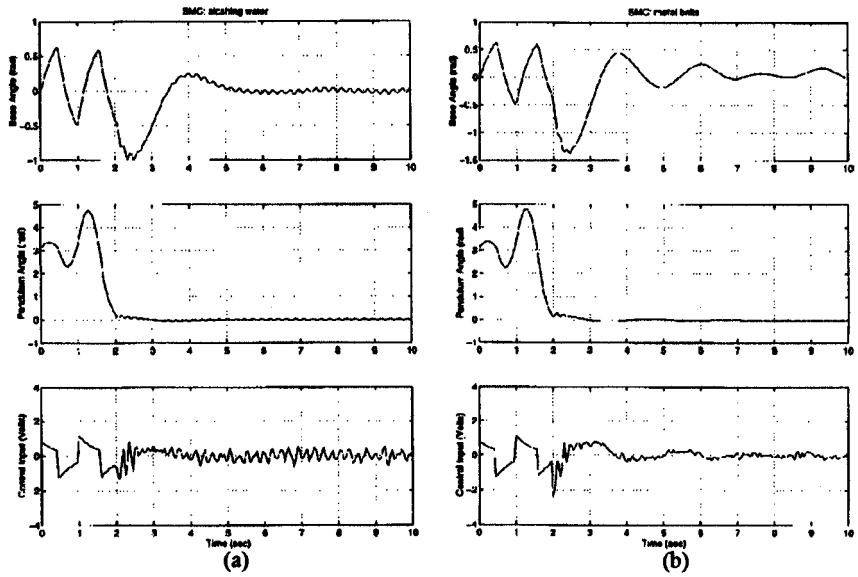

FIGURE 2.3 Rotational inverted pendulum experimental results where (a) water (b) bolts was/were attached to the end of pendulum.

3 ESTIMATION AND CONTROL OF SENSORLESS INDUCTION MOTORS USING SLIDING MODE

For the sake of cost reduction and maintainability, control of an induction motor (IM) without mechanical sensors receives wide attention in both fields-electric drive and dynamic control. This section addresses a new closed loop approach to estimate IM speed as well as rotor time constant for speed/torque sensorless control. Under commonly used assumptions the motion equations of an IM may be partitioned into three categories. First of all, the rotor mechanical system

$$\frac{\mathrm{d}n}{\mathrm{d}t} = \frac{P}{J}(T - T_l), \quad T = \frac{3P}{2}\frac{L_m}{L_r}(i_\beta \lambda_\alpha - i_\alpha \lambda_\beta), \tag{3.1}$$

second, the rotor flux equations,

$$\frac{\mathrm{d}\lambda_\alpha}{\mathrm{d}t} = -\eta\lambda_\alpha - \omega\lambda_\beta + \eta L_m i_\alpha, \quad \frac{\mathrm{d}\lambda_\beta}{\mathrm{d}t} = -\eta\lambda_\beta - \omega\lambda_\alpha + \eta L_m i_\beta \tag{3.2}$$

and, finally, the stator current dynamics,

$$\begin{aligned} \frac{\mathrm{d}i_\alpha}{\mathrm{d}t} &= -\beta\eta\lambda_\alpha + \beta\omega\lambda_\beta - \left(\frac{R_S}{\sigma L_S} + \beta\eta L_m\right) i_\alpha + \frac{1}{\sigma L_S} u_\alpha \\ \frac{\mathrm{d}i_\beta}{\mathrm{d}t} &= -\beta\eta\lambda_\beta + \beta\omega\lambda_\alpha - \left(\frac{R_S}{\sigma L_S} + \beta\eta L_m\right) i_\beta + \frac{1}{\sigma L_S} u_\beta, \end{aligned} \tag{3.3}$$

where stator voltage or current vector (f_α, f_β), defined by their phase vectors (f_a, f_b, f_c) as

$$\begin{bmatrix} f_\alpha \\ f_\beta \end{bmatrix} = \frac{2}{3}\begin{bmatrix} 1 & -1/2 & -1/2 \\ 0 & 3^{1/2}/2 & -3^{1/2}/2 \end{bmatrix}\begin{bmatrix} f_a \\ f_b \\ f_c \end{bmatrix} \tag{3.4}$$

A summary of the parameters, variables may be found in the following Table I. More details may be found in the paper [8].

The objective is to design an observer to estimate motor speed and rotor time constant simultaneously under the assumption that they are constant. First, the sliding mode observer for current is designed

$$\begin{aligned} \frac{d\hat{i}_\alpha}{dt} &= -\frac{R_S}{\sigma L_S}\hat{i}_\alpha + \frac{1}{\sigma L_S}u_\alpha + V_\alpha \\ \frac{d\hat{i}_\beta}{dt} &= -\frac{R_S}{\sigma L_S}\hat{i}_\beta + \frac{1}{\sigma L_S}u_\beta + V_\beta \end{aligned} \tag{3.5}$$

where $\hat{i}_{\alpha/\beta}$ are estimated stator current components, $V_{\alpha/\beta}$ are discontinuous functions of the stator current mismatches

$$\begin{aligned} V_\alpha &= -V_0 \operatorname{sgn}(\hat{i}_\alpha - i_\alpha) \\ V_\beta &= -V_0 \operatorname{sgn}(\hat{i}_\beta - i_\beta). \end{aligned} \tag{3.6}$$

The equivalent values of discontinuous functions $V_{\alpha/\beta}$ are

$$\begin{aligned} [V_\alpha]_{\text{eq}} &= \beta\eta\lambda_\alpha + \beta\omega\lambda_\beta - \beta\eta L_m i_\alpha \\ [V_\beta]_{\text{eq}} &= \beta\eta\lambda_\beta - \beta\omega\lambda_\alpha - \beta\eta L_m i_\beta \end{aligned} \tag{3.7}$$

after sliding mode occurs on the surfaces $s_{\alpha/\beta} = \hat{i}_{\alpha/\beta} - i_{\alpha/\beta} = 0$. These equivalent values may be obtained equating derivatives of current observation mismatches to zero. By our assumption $\dot{\omega} = 0$ and $\dot{\eta} = 0$ which imply that mechanical process and rotor resistance heating are much slower than currents and flux variations.

Denote the equivalent values of $V_{\alpha/\beta}$ by $L_{\alpha/\beta}$. As follows from (3.7),

$$\dot{L}_\alpha = \beta\eta\dot{\lambda}_\alpha + \beta\omega\dot{\lambda}_\beta - \beta\eta L_m \dot{i}_\alpha, \quad \dot{L}_\beta = \beta\eta\dot{\lambda}_\beta - \beta\omega\dot{\lambda}_\alpha - \beta\eta L_m \dot{i}_\beta \tag{3.8}$$

TABLE I Nomenclature of a Induction Motor Model (3.1)–(3.3).

Parameters	*Explanation*	*Parameters*	*Explanation*
$i_{k=a,b}$	Phase currents in (α, β) coordinate	$u_{m=a,b}$	Phase voltages in (α, β) coordinate
$i_{k=a,b,c}$	Phase currents	$u_{m=a,b,c}$	Phase voltages
$\omega/\lambda_{\alpha/\beta}$	Rotor speed/Flux	η	Rotor time constant
T_l	Load torque	T	Torque developed by IM
J	Inertia	σ, β	Leakage parameters
R_r, R_S	Rotor/Stator resistances	P	Number of pole pairs
L_r, L_S	Rotor/Stator inductances	L_m	Mutual inductance

which leads to

$$\dot{\lambda}_\alpha = -\frac{L_\alpha}{\beta}, \quad \dot{\lambda}_\beta = -\frac{L_\beta}{\beta} \tag{3.9}$$

along with the Eqs. (3.2) and (3.7). From (3.8) we may elaborate an intermediate asymptotic observer for $L_{\alpha/\beta}$

$$\begin{bmatrix} \dot{\hat{L}}_\alpha \\ \dot{\hat{L}}_\beta \end{bmatrix} = -\begin{bmatrix} \hat{\eta} & \hat{\omega} \\ -\hat{\omega} & \hat{\eta} \end{bmatrix}\begin{bmatrix} L_\alpha \\ L_\beta \end{bmatrix} - \beta\hat{\eta}L_m\begin{bmatrix} i_\alpha \\ i_\alpha \end{bmatrix} - K\begin{bmatrix} \bar{L}_\alpha \\ \bar{L}_\beta \end{bmatrix}, \tag{3.10}$$

where K is a positive constant to be selected, $\bar{L}_{\alpha/\beta}$ are mismatches between estimation $\hat{L}_{\alpha/\beta}$ and $L_{\alpha/\beta}$ from (3.7), $\hat{\eta}$ and $\hat{\omega}$ are estimation of η and ω. From (3.8), (3.9) and (3.10) the error dynamics of the proposed observer may be represented in the form

$$\begin{bmatrix} \dot{\bar{L}}_\alpha \\ \dot{\bar{L}}_\beta \end{bmatrix} = -\begin{bmatrix} \bar{\eta} & \bar{\omega} \\ -\bar{\omega} & \bar{\eta} \end{bmatrix}\begin{bmatrix} L_\alpha \\ L_\beta \end{bmatrix} - \beta\bar{\eta}L_m\begin{bmatrix} i_\alpha \\ i_\alpha \end{bmatrix} - K\begin{bmatrix} \bar{L}_\alpha \\ \bar{L}_\beta \end{bmatrix}, \tag{3.11}$$

To ensure the convergence of $\bar{\eta} = \hat{\eta} - \eta$ and $\bar{\omega} = \hat{\omega} - \omega$ to zero we choose the adaptation law

$$\begin{bmatrix} \dot{\bar{\eta}} \\ \dot{\bar{\omega}} \end{bmatrix} = -\begin{bmatrix} L_\alpha + \beta L_m i_\alpha & L_\beta + \beta L_m i_\beta \\ L_\beta & -L_\alpha \end{bmatrix}\begin{bmatrix} \bar{L}_\alpha \\ \bar{L}_\beta \end{bmatrix}, \tag{3.12}$$

based on the Lyapunov function

$$V = \frac{1}{2}\bar{L}_\alpha^2 + \frac{1}{2}\bar{L}_\alpha^2 + \frac{1}{2}\bar{\eta}_\alpha^2 + \frac{1}{2}\bar{\omega}_\alpha^2. \tag{3.13}$$

It can be shown that $\bar{L}_{\alpha/\beta}$ of (3.11) tends to zero and

$$\begin{bmatrix} L_\alpha + \beta L_m i_\alpha & L_\beta \\ L_\beta + \beta L_m i_\beta & -L_\alpha \end{bmatrix}\begin{bmatrix} \bar{\eta} \\ \bar{\omega} \end{bmatrix} = \begin{bmatrix} 0 \\ 0 \end{bmatrix}. \tag{3.14}$$

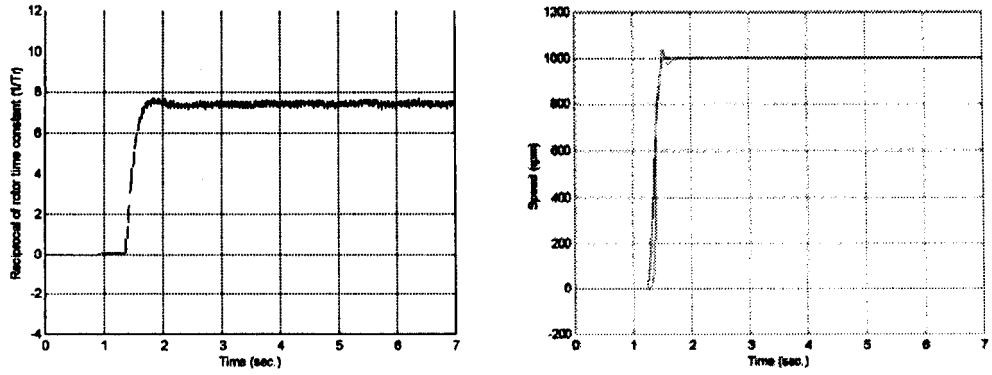

FIGURE 3.1 (Left) Rotor constant estimation. (Right) Estimated (dashed-line) and measured (solid-line) IM speed.

If i_α and i_β are linearly independent (which is common for IM) then $\bar{\eta} = 0$ and $\bar{\omega} = 0$ or the estimated rotor constant and speed tend to real ones, $\hat{\eta} \to \eta$ and $\hat{\omega} \to \omega$. Details of the above proof may be found again in [8]. The proposed observation algorithm was implemented on the test bed of OSU PEEM (Power Electronic and Electric Machines) Lab and results may be found in the following Figure 3.1, which demonstrates the proposed estimation algorithm's capability to estimate the rotor constant and IM rotor speed simultaneously.

4 BACK ELECTROMOTIVE FORCE (EMF) ESTIMATOR FOR AUTOMOTIVE ALTERNATOR

One of the modern approaches used in automobile industry to optimizing the efficiency of today's three-phase alternator is to employ a controllable rectifier through the six-step switching algorithm [1]. The vital information needed for the rectifier to switch from one to another is acquired by detecting the alternator's back electromotive forces (EMFs). Usually the back EMFs may be found if the rotor position is measured which is widely employed now. For the sake of cost reduction and maintainability a sliding mode observer is designed to estimate the necessary information, back EMF, for the rectifier's switching algorithm utilizing both the battery current and voltage measurement, which is readily available. Basically, the dynamics of a three-phase generator may be described in the following four equations:

$$\begin{aligned}
\frac{di_1}{dt} &= -\frac{R_\omega}{L} i_1 - \frac{\upsilon_0}{6L}(2u_1 - u_2 - u_3) + \frac{1}{L} e_1(t) \\
\frac{di_2}{dt} &= -\frac{R_\omega}{L} i_2 - \frac{\upsilon_0}{6L}(2u_2 - u_1 - u_3) + \frac{1}{L} e_2(t) \\
\frac{di_3}{dt} &= -\frac{R_\omega}{L} i_3 - \frac{\upsilon_0}{6L}(2u_3 - u_1 - u_2) + \frac{1}{L} e_3(t) \\
\left(\frac{R_L + R_b}{R_L}\right)\frac{du_c}{dt} &= -\frac{1}{R_L C} u_c + \frac{1}{2C}\sum_{i=1}^{3} u_k i_k
\end{aligned} \tag{4.1}$$

Please refer to Table II for the nomenclature of the model parameters.

More details of this model may be found in [2]. Suppose that e_1 (back EMF) of phase 1 may be found based on the measurement of battery current i_{battery} (see Fig. 4.1). It can be done if link current coincide with phase current i_1. It happens in so-called "observation window" when S_1, S_5 and S_6 (or S_2, S_3 and S_4) are closed or $u_1 \neq u_2 = u_3$.

We assume that the following ramp function an acceptable model of the time-varying engine speed:

$$\omega = \alpha t + \beta \tag{4.2}$$

Then back EMF may be found as

$$e_1 = -A_{\text{amp}}(\alpha t + \beta)\sin\left(\frac{\alpha}{2} t^2 + \beta t + \gamma\right) \tag{4.3}$$

where α is acceleration and β, γ are constants.

TABLE II Nomenclature of a Three-phase Generator Model (4.1).

Parameters	*Explanation*	*Parameters*	*Explanation*
$i_{k=1,2,3}$	Phase currents	$u_{m=1,2,3}$	Switching signals (+1 or −1)
R_ω	Winding resistance	u_c	Voltage of capacitor
R_L	Load resistance	v_o	DC output voltage
R_b	Battery resistance	C	Battery resistor
L	Winding inductance	$e_{m=1,2,3}$	Back EMFs

To estimate the load current, the following observer is proposed based on the readily available battery current

$$\frac{\mathrm{d}\hat{i}_1}{\mathrm{d}t} = -\frac{R_\omega}{L}\hat{i}_1 - \frac{v_0}{6L}(2u_1 - u_2 - u_3) + \frac{1}{L}e_1(t) + \frac{1}{L}M_1\mathrm{sgn}(u_1 i_{\text{battery}} - \hat{i}_1). \tag{4.4}$$

Denote the sliding surface as

$$s_1 = u_1 i_{\text{battery}} - \hat{i}_1. \tag{4.5}$$

Since $u_1 i_{\text{battery}} = i_1$ within the observation window when $u_1 \neq u_2 = u_3$ and $i_{\text{battery}} = i_{\text{link}} - i_{\text{load}}$, the derivative of s_1 is of the form

$$\begin{aligned}\dot{s}_1 &= \frac{\mathrm{d}}{\mathrm{d}t}i_1 - u_1\frac{\mathrm{d}}{\mathrm{d}t}i_{\text{load}} - \frac{\mathrm{d}}{\mathrm{d}t}\hat{i}_1 \\ &= -\frac{1}{L}\left[R_\omega s_1 - e_1 + M_1\mathrm{sgn}(s_1) + R_\omega u_1 i_{\text{load}} + u_1 L\frac{\mathrm{d}}{\mathrm{d}t}i_{\text{load}}\right].\end{aligned} \tag{4.6}$$

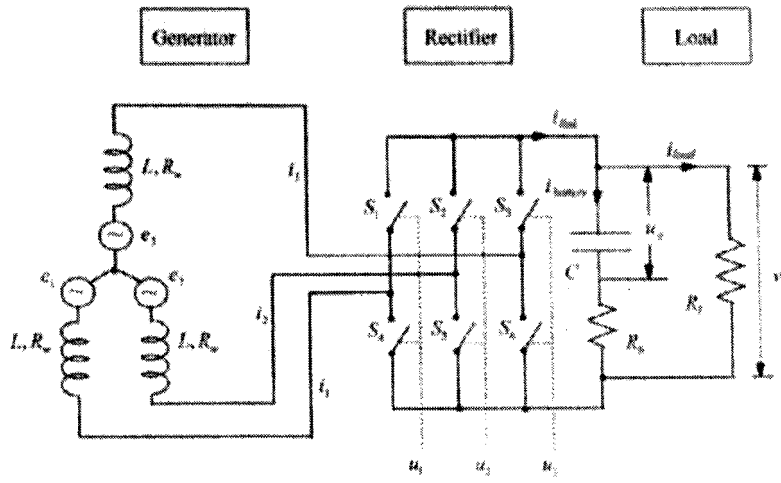

FIGURE 4.1 Schematic diagram of automotive.

In sliding mode on the surface $s_1 = u_1 i_{\text{battery}} - \hat{i}_1 = 0$ the average value of $M_1 \operatorname{sgn}(s_1)$ found by a low pass filter [2] is of the following form

$$z = [M_1 \operatorname{sgn}(s_1)]_{\text{eq}} = \left[e_1 - R_\omega u_1 i_{\text{load}} - u_1 L \frac{\mathrm{d}}{\mathrm{d}t} i_{\text{load}} \right]. \tag{4.7}$$

Denoting $q = 1/R_L$ (4.7) may be represented as

$$\left[e_1 - R_\omega u_1 i_{\text{load}} - u_1 L \frac{\mathrm{d}}{\mathrm{d}t} i_{\text{load}} \right] = \left[e_1 - u_1 \frac{1}{R_L} \left(R_\omega \upsilon_0 + L \frac{\mathrm{d}}{\mathrm{d}t} \upsilon_0 \right) \right] = e_1 - u_1 q h(t). \tag{4.8}$$

where $\upsilon_0 = i_{\text{load}} \cdot R_L$. In (4.8) the function $h(t)$ is

$$h(t) = i_{\text{load}} - L \frac{\mathrm{d}}{\mathrm{d}t} i_{\text{load}}. \tag{4.9}$$

and the parameter R_L is considered as unknown constant, $\dot{R}_L = 0$, here to embrace the fact of parameter variation. Note that DC output voltage υ_0 is available and its derivative may be found from

$$\frac{\mathrm{d}}{\mathrm{d}t} \upsilon_0 = \frac{1}{C} i_{\text{battery}} + R_{\text{battery}} \frac{\mathrm{d}}{\mathrm{d}t} i_{\text{battery}}. \tag{4.10}$$

In addition the battery current is readily available and its derivative may be found from

$$\frac{\mathrm{d}}{\mathrm{d}t} i_{\text{battery}} = -\frac{R_\omega}{L} i_{\text{battery}} - \frac{\upsilon_0}{6L} (2u_1 - u_2 - u_3) + \frac{1}{L} M_1 \operatorname{sgn}(s_1). \tag{4.11}$$

Therefore, the function $h(t)$ may be found from (4.9)

Introduce a new variable

$$z = e_1 - u_1 q h(t). \tag{4.12}$$

Now, with the measurement of engine speed ω and known function $h(t)$, a 5th-order nonlinear asymptotic observer is proposed to estimate back EMF e_1 unknown load current and unknown constant q simultaneously:

$$\begin{aligned}
\dot{\hat{e}}_1 &= \hat{e}'_1 - L_{11}[\hat{e}_1 - (z + u_1 \hat{q} h(t))] \\
\dot{\hat{e}}'_1 &= -\left(\hat{\omega}^2 + \frac{3\hat{\alpha}^2}{\hat{\omega}^2} \right) \hat{e}_1 - \frac{3\hat{\alpha}^2}{\hat{\omega}^2} \hat{e}'_1 - L_{21}[\hat{e}_1 - (z + u_1 \hat{q} h(t))] \\
\dot{\hat{\omega}} &= \hat{\alpha} - L_{31}(\hat{\omega} - \omega) \\
\dot{\hat{\alpha}} &= -L_{41}(\hat{\omega} - \omega) \\
\dot{\hat{q}} &= L_{51} u_1 ([\hat{e}_1 - (z + u_1 \hat{q} h(t))])
\end{aligned} \tag{4.13}$$

Simulation results may be found in Figure 4.2 where the proposed observer demonstrates its capability of estimating unknown constant q (upper-right of Fig. 4.2), load current i_{load} (lower-right of Fig. 4.2) and back EMF (upper/lower-left of Fig. 4.2).

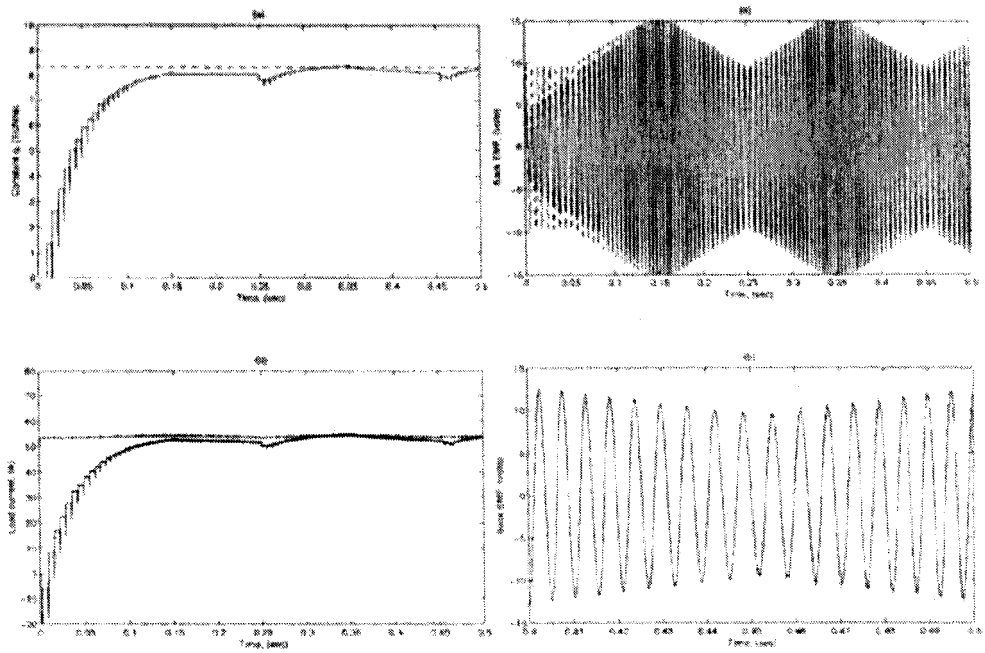

FIGURE 4.2 Estimation results of unknown constant q, load current i_{load} and back EMF.

5 NO_x CONTROL FOR EGR–VGT DIESEL ENGINE

Exhaust gas recirculation (EGR) combined with the variable geometry turbocharging provides an important avenue for NO_x emission reduction. In this section we study the problem of EGR–VGT control from the sliding mode design perspective. The departure point for our work is the reduced order model in [10] that we use for the control design:

$$\dot{p}_1 = k_1\left[\frac{\eta_C}{T_a C_p}\frac{P_C}{((p_1/p_a)^{\mu}-1)} - k_e p_1 + W_{\text{egr}}\right], \tag{5.1}$$

$$\dot{p}_2 = k_2(k_e p_1 + W_f^d - W_{\text{egr}} - u_{2t}), \tag{5.2}$$

$$\dot{P}_C = -\frac{1}{\tau}\left[P_C - \eta_m \eta_t T_2 C_p\left(1 - \left(\frac{p_a}{p_2}\right)^{\mu}\right)u_{2t}\right], \tag{5.3}$$

where:

p_1/p_2: intake/exhaust manifold pressure.
P_C: compressor power.
k_e: pumping rate constant,
W_{egr}: EGR flow rate which is equal to u_{12} or u_{21},
η_C, η_t: compressor and turbine isentropic efficiencies,
η_m: turbocharger mechanical efficiency,
τ: turbine-to-compressor power transfer time constant,
C_p, C_V: specific heats at constant pressure, volume.

To account for the fact that the turbine cannot immediately realize the commanded air flow because of the actuator dynamics, a first order linear system is introduced as

$$\dot{u}_{2t} = -\frac{1}{\tau_A} u_{2t} + \frac{1}{\tau_A} v_{2t}, \tag{5.4}$$

where

τ_A: time constant,
v_{2t}: commanded VG turbine flow rate, that is achieved in steady-state.

Controlling only p_2 or P_C may result in either unstable zero dynamics or slow rate of convergence. To cope with this problem, first of all, desired system states are selected based on some specific operating points and the problem is then redefined as a stabilization one with states Δp_1, Δp_2 and ΔP_C, the difference between desired and actual one. Following the approach in [11], a new variable is found by solving an appropriate partial differential equation such that the system may be reduced to the regular form. This variable is

$$\phi_{\Delta P_C} = \Delta P_C + \frac{\eta_m \eta_t T_2 C_p}{k_2 \tau} \left[\Delta p_2 - \frac{p_a^\mu}{1-\mu} (\Delta p_2 + p_{2\text{des}})^{1-\mu} + \frac{p_a^\mu}{1-\mu} (p_{2\text{des}})^{1-\mu} \right]. \tag{5.5}$$

This new variable has the property that $\dot{\phi}_{\Delta P_C}$ does not depend explicitly on the control input. The system in the regular form is

$$\Delta \dot{p}_1 = k_1 \left[-k_e \cdot (\Delta p_1 + p_{1\text{des}}) + \frac{\eta_c}{T_a C_p} \frac{\phi_{\Delta P_c} + (**)}{(\Delta p_1 + p_{1\text{des}}/p_a)^\mu - 1} + W_{\text{egr}} \right] \tag{5.6}$$

where

$$(**) = P_C^d - \frac{\eta_m \eta_t T_2 C_p}{k_2 \tau} \left[\Delta p_2 - \frac{p_a^\mu}{1-\mu} (\Delta p_2 + p_{2\text{des}})^{1-\mu} + \frac{p_a^\mu}{1-\mu} (p_{2\text{des}})^{1-\mu} \right].$$

$$\begin{aligned} \dot{\phi}_{\Delta P_C} = & -\frac{1}{\tau} \phi_{\Delta P_C} - \frac{1}{\tau} P_C^d \\ & + \frac{\eta_m \eta_t T_2 C_p}{k_2 \tau^2} \left\{ \begin{array}{l} \Delta p_2 + \dfrac{p_a^\mu}{\mu - 1} [(\Delta p_2 + p_{2\text{des}})^{1-\mu} - (p_{2\text{des}})^{1-\mu}] \\ + k_2 \tau \left[1 - \left(\dfrac{p_a}{\Delta p_2 + p_{1\text{des}}} \right)^\mu \right] [k_e (\Delta p_1 + p_{1\text{des}}) + W_f^d - W_{\text{egr}}] \end{array} \right\} \end{aligned} \tag{5.7}$$

$$\Delta \dot{p}_2 = k_2 [k_e (\Delta p_1 + p_{1\text{des}}) + W_f^d - W_{\text{egr}}] - k_2 (u_2 + u_{2\text{des}}) \tag{5.8}$$

Note that the control u_2 explicitly affects only (5.8). The EGR flow rate, W_{egr}, is treated as an external input to these equations as it is controlled by a separate controller.

The state variable, Δp_2, involved in the Eq. (5.7) may be treated as a fictitious control input,

$$\Delta p_2 = -K_S \cdot \phi_{\Delta P_C}, \quad K_S > 0, \tag{5.9}$$

to speed up the dynamics of the state, $\phi_{\Delta P_C}$. This relationship can be held by enforcing the sliding mode on the surface,

$$s = \Delta p_2 + K_S \cdot \phi_{\Delta P_C} = 0. \tag{5.10}$$

With the actuator dynamics (5.4) included, the relative degree of the system from u_2 to s increases by one and the proposed control algorithm is not directly applicable. What we can do, however, is to modify the sliding surface as

$$S = \dot{s} + \alpha \cdot s, \quad \alpha > 0, \tag{5.11}$$

where

$$\begin{aligned} \dot{s} = \dot{p}_2 &\left[1 + K_S \frac{T_2 \eta_{tm} \eta_{\text{tuis}} c_p}{\tau_{tc} k_2} \left(1 - \left(\frac{p_{\text{atm}}}{p_2}\right)^{\mu}\right)\right] - \frac{K_S P_C}{\tau_\kappa} \\ &+ K_S \frac{T_2 \eta_{tm} \eta_{\text{tuis}} C_p}{\tau_{tc} k_2} \left(1 - \left(\frac{p_{\text{atm}}}{p_2}\right)^{\mu}\right)(u_2 + u_{2\text{des}}) \end{aligned} \tag{5.12}$$

and α determines the rate of decay for s (after the sliding mode is enforced). The control v_{2t}, is then developed to enforce the sliding mode on the surface (5.11). The control algorithm and observer for its implementation are described in [12]. The actual control input is implemented as a discontinuous function

$$u_2 = M \cdot \text{sgn}(S). \tag{5.13}$$

The performance of the proposed SM control is examined by simulation. The controller parameters, (K_S, α and M), were determined from the simulations of the reduced order model augmented with VGT actuator dynamics. The EGR flow rate W_{egr} is assumed to be generated

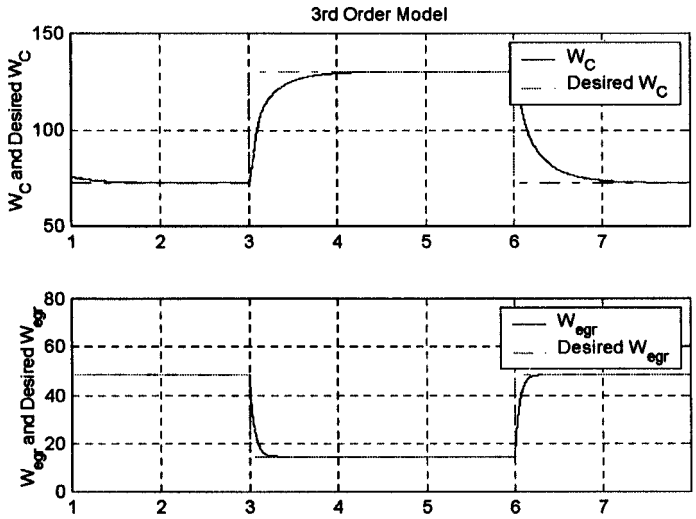

FIGURE 5.1 Desired versus regulated values of compressor mass flow rate and EGR mass flow rate.

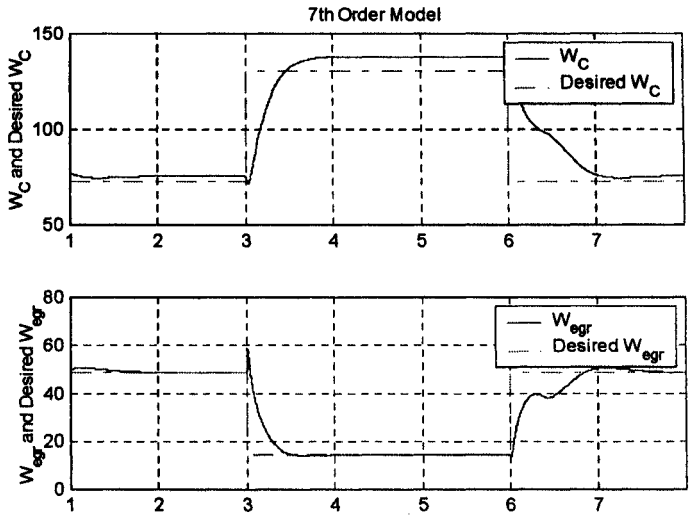

FIGURE 5.2 Closed loop responses on the higher order (7th-order) model.

by a first order lag with the steady-state value of W^d_{egr}. The closed loop responses are illustrated in the following Figure 5.1.

The same controller with the same set-points was applied to the more accurate, higher order model [10] and acceptable performance has been observed in Figure 5.2. Note that, for the scenario of higher order model, the EGR flow was generated by assuming that the EGR valve position is driven by a first order lag towards the desired position. The non-monotonic character of EGR flow response is due to the dependence of this flow on intake and exhaust manifold pressures.

6 AUTOMOBILE CLIMATE CONTROL USING SLIDING MODE

In this section a temperature regulation problem for an automotive air conditioning system with Electronic Variable Compressor (EVC) will be studied. Note that the capacity EVC is indirectly regulated by the pressure difference of crankcase and suction port through the electronically controlled Valve Duty Cycle (VDC).

The climate control system consists of several components such as condenser, orifice tubes, evaporator, refrigerant accumulator and electronic variable compressor. The motion equations may be partitioned into two groups.

First group consists of the Refrigerant Cycle subsystem

$$\dot{P}_d = \frac{1}{C_1}\left[Q - \frac{P_d - P_{\text{cond}}}{R_1}\right], \quad \dot{P}_{\text{cond}} = \frac{1}{C_2}\left[\frac{P_d - P_{\text{cond}}}{R_1} - \frac{P_{\text{cond}} - P_{\text{evap}}}{R_2}\right],$$
$$\dot{P}_{\text{evap}} = \frac{1}{C_3}\left[\frac{P_{\text{cond}} - P_{\text{evap}}}{R_2} - \frac{R_{\text{evap}} - P_S}{R_3}\right],$$

$$\dot{P}_S = \frac{1}{C_4}\left[\frac{P_{\text{evap}} - P_S}{R_3} - Q\right], \quad \dot{T}_{\text{airout}} = \frac{K_6 P_{\text{evap}} - T_{\text{airout}}}{\tau_4}, \tag{6.1}$$

and the second one that describes the behaviors of EVC

$$\begin{aligned}
\dot{P}_{CC} &= \frac{-P_{CC} + \mathrm{VDC} \cdot P_d + (1 - \mathrm{VDC})P_S}{\tau}, \\
\ddot{x} &= -\frac{B}{M}\dot{x} - \frac{K}{M}x + \frac{L_2 \cdot 2A_{\mathrm{piston}}}{R_1 M}(P_S - P_{CC} + P_{\mathrm{fric}}) \\
&\quad + \frac{L_3 A_{\mathrm{piston}}}{L_1 M}(P_d - P_S + 2P_{CC}), \quad P_{\mathrm{fric}} = P_0 \cdot \mathrm{sgn}(\dot{x}) \\
Q &= K_{\mathrm{flow}}(N) \cdot x (N \text{ is measurable compressor speed}).
\end{aligned} \tag{6.2}$$

Nomenclature for (6.2) may be found in Table III.

According to the motion equations, the refrigerant flow rate, Q, may be considered as the intermediate control input of the block describing refrigerant cycle subsystem. Next, the flow rate may be regulated by proper VDC control action according to the nonlinear compressor dynamics.

To assign desired refrigerant flow rate Q we consider first the refrigerant cycle subsystem (6.1). The eigenvalues of (6.1) differ considerably and the dynamics of P_d, P_{cond} and P_{evap} dynamics may be disregarded because they are all stable. Instead of conventional eigenvalue assignment method the intermediate control design Q for this multi-rate system may be decoupled into the following steps:

1. The Zero Dynamics of the refrigerant system (marked by dashed line), if considering P_{evap} as the system output, are stable which implies that we may control P_{evap} rather than all the states of the multi-rate system (6.1).
2. Since the dynamics of T_{airout} determined by τ_4 are acceptable, one may regulate the temperature to desired one considering P_{evap} as a fictitious control.
3. Assume the desired P_{evap} may be assigned as $P^*_{\mathrm{evap}} = T_{\mathrm{des}}/K_6$. As a result the last equation of (6.1) becomes

$$\dot{T}_{\mathrm{airout}} = \frac{K_6 P_{\mathrm{evap}} - T_{\mathrm{airout}}}{\tau_4} = \frac{K_6(T_{\mathrm{des}}/K_6) - T_{\mathrm{airout}}}{\tau_4}, \quad \tau_4 > 0,$$

which implies $T_{\mathrm{airout}} \to T_{\mathrm{des}}$ at the rate of K_6/τ_4. T_{des} is the set-point of evaporator out temperature.

TABLE III Nomenclature of an Automotive Air Conditioning System (6.1) and (6.2).

Parameters	*Explanation*	*Parameters*	*Explanation*
P_d	Discharge pressure	P_{cond}	Condenser pressure
P_{evap}	Evaporator pressure	P_0	Friction magnitude
P_S	Suction pressure	x	Compressor stroke
P_{CC}	Crank case pressure	T_{airout}	Evaporator out temperature
P_{fric}	Friction in terms of pressure	VDC	Valve Duty Cycle (Actual control action)
N	Engine speed	Q	Refrigerant flow rate

4. From the last second and third equations of (6.1), the desired refrigerant flow Q for refrigerant cycle may be selected as

$$Q_{\text{desired}} = x_{\text{des}} \cdot K_{\text{flow}} = (C_3 + C_4)[\Gamma^* + K(P_{\text{evap}} - P^*_{\text{evap}})],$$
$$\Gamma^* = \frac{1}{C_3 + C_4}\left[\frac{P_{\text{cond}} - P_{\text{evap}}}{R_2}\right],$$

such that the $P_{\text{evap}} \to P^*_{\text{evap}}$ tends to the desired one. This design may be verified by substituting Q_{desired} into P_{evap} dynamics.

5. The rate of $P_{\text{evap}} \to P^*_{\text{evap}}$ is determined by K after desired Q_{desired} is assigned.

Next, we may calculate desired crank case pressure which makes EVC generate desired refrigerant flow rate Q_{desired}

$$(P_{\text{CC}})_{\text{des}} = \frac{[(2L_2 - L_3)P_S + L_3P_d + L_2P_{\text{fric}} - ((L_1K_{\text{comp}})/A_{\text{piston}})x_{\text{des}}]}{2(L_2 - L_3)} \tag{6.3}$$

which may be derived from the second equation of EVC dynamics (6.2) assuming the subsystem is stable. Note that x_{des} in (6.3) implies the desired refrigerant flow rate $Q_{\text{desired}}(Q_{\text{desired}} = x_{\text{des}} \cdot K_{\text{flow}})$.

Since the desired crank case pressure may be evaluated, the discontinuous control action of compressor (indeed, VDC) as a continuous state function by selecting the slope k and small region ε

$$\text{VDC}(k \cdot S + \text{bias}) = \begin{cases} (k \cdot S + \text{bias}) & \text{if } |(k \cdot S + \text{bias})| \le \varepsilon \\ 1.0 & \text{if } (k \cdot S + \text{bias}) > \varepsilon \\ 0.0 & \text{if } (k \cdot S + \text{bias}) < -\varepsilon, \end{cases} \tag{6.4}$$
$$S = P_{\text{CC}} - (P_{\text{CC}})_{\text{des}},$$

where bias = 0.5 because VDC may only vary from 0 to 1. Note that $S = 0$ is the switching surface. A plot of this function may be seen below (Fig. 6.1)

For different sensor availability scenarios different observers are designed to acquire necessary information for controller. See [16] for more details about observer design. Numerical simulation is performed to regulate evaporator out temperature to 50 °F and result is demonstrated in the following Figure 6.2. Basically, smooth crank case pressure curve implies smooth control action which is another requirement for climate controller.

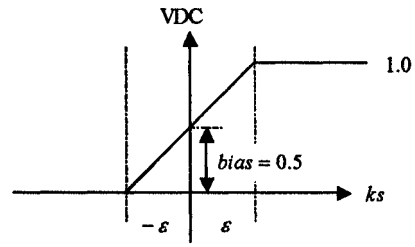

FIGURE 6.1 Schematic diagram of function (6.4).

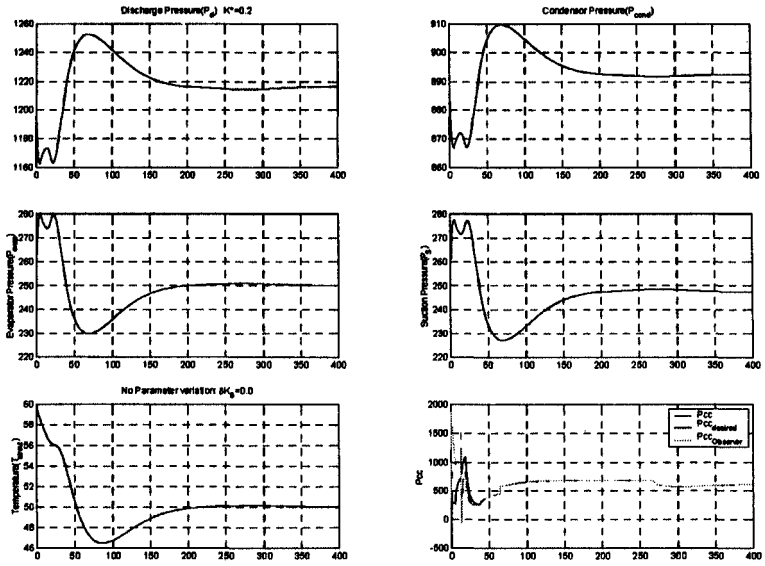

FIGURE 6.2 Temperature (Desired T_{airout} is 50 °F) tracking performance.

7 ESTIMATION WITH BINARY SENSOR USING SLIDING MODE

For a system using a binary sensor where only the sign of the output is available, the conventional observer approach is no longer valid. For such a system, a new observer design approach is explored to provide a guaranteed convergence of the observer. Consider a system with a scalar output y, the sign of the state cx in

$$\begin{aligned} \dot{x} &= Ax + Bu \\ y &= \operatorname{sgn}(cx). \end{aligned} \tag{7.1}$$

It is assumed that input u is such that cx varies its sign in any time interval (t, ∞). Let z_k be the states at sensor switching instants and τ_k be the interval between switching instants:

$$z_k = x(t_k) \quad \text{and} \quad \tau_k = t_k - t_{k-1} \tag{7.2}$$

If the z_k's are known exactly for the entire process, the states in time between t_k and t_{k+1} may be evaluated

$$x(t) = e^{A(t-\tau_k)} z_k + \int_{t_k}^{t} e^{A(t-\tau)} Bu(\tau)\, d\tau. \tag{7.3}$$

However, if it is known only that for any time t_k the value $cz_k = 0$, $t_k < t < t_{k+1}$, that is the case with the binary sensor measurement, then a discrete-time observer is needed to estimate

the discrete sequences z_k. Then, the continuous-time states $x(t)$ may be found using (7.3). The discrete-time observer for z_k can be constructed in the form

$$\hat{z}_k = e^{A\tau_{k-1}}\hat{z}_{k-1} + \int_{t_{k-1}}^{t_k} e^{A(t-\tau)}Bu(\tau)\,d\tau + L_{k-1}(c\hat{z}_{k-1} - cz_{k-1}) \tag{7.4}$$

The selection of the vector gain L_{k-1} for this type of observer is not a trivial task since the system in question is time-varying (because the sensor switching interval τ_k varies in time). For notational simplicity (7.4) may be represented in the following format

$$\hat{z}_k = F_{k-1}\hat{z}_{k-1} + G_{k-1}\{u(t)\}_{t_{k-1}}^{t_k} + L_{k-1}(c\hat{z}_{k-1} - cz_{k-1}) \tag{7.5}$$

where $F_{k-1} = e^{A\tau_{k-1}}$ and $G_{k-1}\{u(t)\}_{t_{k-1}}^{t_k} = \int_{t_{k-1}}^{t_k} e^{A(t-\tau)}Bu(\tau)\,d\tau$.

To provide convergence of the observer in general cases, a deadbeat observer structure is selected with transformation of the system into a specific canonical system representation. Transform the system as

$$w_k = \tilde{F}_{k-1}w_{k-1} + \tilde{G}_{k-1}\{u(t)\}_{t_{k-1}}^{t_k} \tag{7.6}$$

with transformation matrix T

$$w_{k-1} = T_{k-1}x_{k-1}, \quad \tilde{F}_{k-1} = T_{k-1}F_{k-1}T_{k-1}^{-1}, \quad \tilde{G}_{k-1}\{u(t)\}_{t_{k-1}}^{t_k} = G_{k-1}\{u(t)\}_{t_{k-1}}^{t_k}T_{k-1}^{-1} \tag{7.7}$$

such that the system transition matrix has the following structure

$$\tilde{F}_{k-1} = \begin{bmatrix} 0 & \cdots & \cdots & 0 & f_{1k-1} \\ 1 & \ddots & 0 & 0 & f_{2k-1} \\ \vdots & 1 & 0 & 0 & f_{3k-1} \\ 0 & 0 & 1 & \ddots & \vdots \\ 0 & 0 & \cdots & 1 & f_{nk-1} \end{bmatrix} \tag{7.8}$$

where the f_{k-1}'s depend on F_{k-1}. Then, the gain L_{k-1} is selected such that the effect of the time varying parameter in the state transition matrix is canceled by feedback, *i.e.*, the deadbeat observer can be designed by selecting the gain L_{k-1} as $L_{k-1} = [-f_{1k-1} \cdots -f_{nk-1}]^T$. The resulting observer has the following structure

$$\hat{w}_k = \tilde{F}_{k-1}\hat{w}_{k-1} + \tilde{G}_{k-1}\{u(t)\}_{t_{k-1}}^{t_k} + L_{k-1}(\hat{w}_{k-1} - w_{k-1}) \tag{7.9}$$

This deadbeat observer converges with n step where n is the dimension of the system. Now the discrete event system is estimated using the observer designed above. The next step is to construct the continuous states between the discrete intervals. Knowing the estimated states at each switching instant, the continuous states (states between switching) can be calculated as described by Eq. (7.3). The proof of convergence for proposed observer may be found in [6].

The developed methodology was applied to air fuel ratio control of combustion engines. Air fuel ratio should be maintained at certain level with high accuracy. Therefore air and fuel flow rate to cylinder should be found. The dependence between injected fuel and fuel injected to cylinder is complicated and depends on condensing and evaporating of fuel

injected into the film. To calculate AFR the mass of fuel should be estimated. We will now demonstrate how it can be done having binary reading sensor only and taking into account its dynamics. Consider the model including fuel dynamic, AFR in the cylinder, delay and sensor dynamics

$$\begin{aligned} \frac{dx_1(\theta)}{d\theta} &= a_1 x_1(\theta) + b_1 u(\theta), \\ \frac{dx_2}{d\theta} &= a_2 x_2(\theta) + a_{12} x_1(\theta - \theta_d) + b_2 u(\theta - \theta_d), \end{aligned} \tag{7.10}$$

where parameters a_1, a_2, b_1, b_2 and a_{12} are known parameters [7]. The first equation describes the fuel film dynamics while the second one is the AFR sensor dynamics with only binary sensor reading. The state variables $x = [x_1 x_2]^T$ are $[\dot{m}_{ff}\ \phi_m]^T$, the fuel film mass rate and air flow rate respectively. Input $u = \dot{m}_{ft}$ is the fuel injection rate. Due to the binary characteristics of exhaust oxygen sensor, the measurement equation becomes

$$y = \text{sgn}(x_2), \tag{7.11}$$

The observer is designed and results of experiment may be found in Figure 7.1. It shows the estimation of the fuel flow rate in fuel film and linear AFR. After initial transient due to the difference in initial conditions, the estimated state converges to the actual states (Fig. 7.1(a)) within a reasonable accuracy except during throttle tip in.

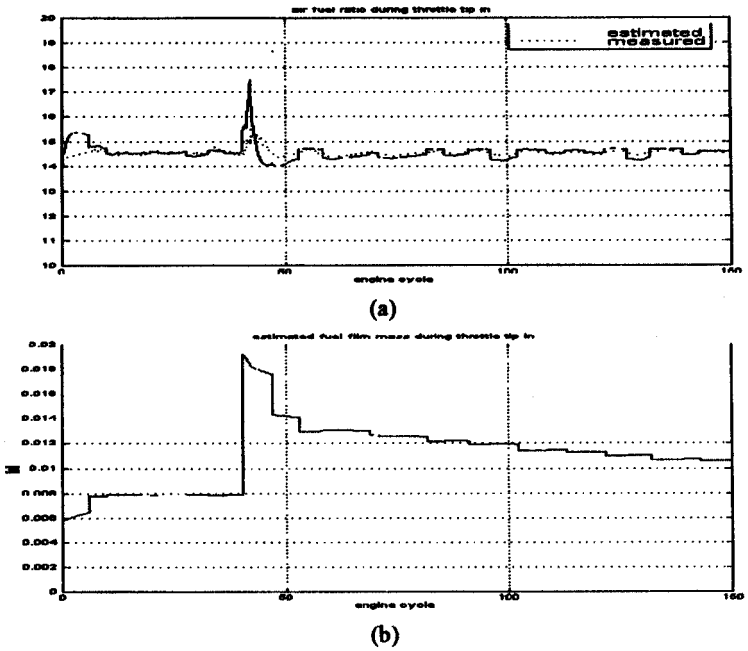

FIGURE 7.1 Observer responses during throttle tip-in: (a) Estimated and measured AFR (b) Estimated fuel film mass.

8 ANTI-LOCK BRAKE SYSTEM (ABS) CONTROL USING SLIDING MODE SELF-OPTIMIZATION

To maximize the braking force ABS controller should be able to maximize the friction coefficient between tires and road surfaces. The friction coefficient depends on the slip rate, the ratio of real and calculated vehicle speed, and this function is unknown and is varying depending on road surface. In this section a sliding mode self-optimization methodology [13, 14] is applied to search the optimal friction gain during the course of braking.

This study is conducted based on the model of longitudinal motion. Assumption is made that right wheels and left wheels have different slip-friction functions and the functions are both unknown. The model consists of two parts: Rotational Dynamics of wheels and Longitudinal Dynamics of vehicle. The following equations of rotational dynamics are derived under the assumption that the engine is disengaged in course of braking:

$$J_w\dot{\omega}_i = R_w F_{ti} - B_t\omega_i - T_{bi}, \quad i = 1, 2, 3, 4 \tag{8.1}$$

where F_{ti}s are tire friction/tractive forces with road and T_{bi}s are braking torque. The governing equations for longitudinal motion are of the form,

$$(M_{\text{car}} + 4{*}m_w) \cdot \dot{V}_L = -F_{t1} - F_{t2} - F_{t3} - F_{t4} - F_o. \tag{8.2}$$

where the nonlinear terms inside (8.2) may be found below:

$$\begin{aligned}
F_a &= C_d A_f V_L^2 \quad \text{(Aerodynamic drag force)} \\
F_{t1} &= N_{\text{front}}\mu(\lambda_1) \quad F_{t2} = N_{\text{front}}\mu(\lambda_2) \quad F_{t3} = N_{\text{rear}}\mu(\lambda_3) \quad F_{t4} = N_{\text{rear}}\mu(\lambda_4) \\
N_{\text{front}} &= \frac{1}{2}\left[\left(1 - \frac{a}{\ell}\right)M_{\text{car}}g - \frac{M_{\text{car}}h_{\text{cg}}}{\ell}\dot{V}_L\right] \quad \text{(Front wheel normal forces)} \\
N_{\text{rear}} &= \frac{1}{2}\left[\left(\frac{a}{\ell}\right)M_{\text{car}}g + \frac{M_{\text{car}}h_{\text{cg}}}{\ell}\dot{V}_L\right] \quad \text{(Rear wheel normal forces)} \\
\lambda_t &= \frac{V_L - R_w\omega_t}{V_L} \quad \text{(Slip rate).}
\end{aligned} \tag{8.3}$$

Details of model variables and parameters may be found in Table IV.

The slip-friction function, $\mu(\lambda_i)$, is unknown and depends only on the road surfaces/conditions. A typical plot of the function may be found in Figure 8.1. Usually, the maximum value of friction is for relative slip $\lambda = 0.2$ for many road conditions. The brake controller should be able to find the optimal coefficient of friction under the fact that the function itself

TABLE IV Nomenclature of Vehicle Model (8.1), (8.2) and (8.3).

Parameters	*Explanation*	*Parameters*	*Explanation*
J_w	Wheel inertia	R_w	Wheel radus
B_t	Viscous friction ratio	m_w	Wheel mass
M_{car}	Vehicle total mass	C_d	Aero drag force coefficient
A_f	Effective frontal are	ℓ	Distance between front and rear wheels
λ_t	Slip rate	$\mu(\lambda_t)$	Coeff. of friction between road and tire
a	Distance from vehicle mass front wheel center	h_{cg}	Height of vehicle mass center
ω_t	Wheel rotational speed	V_L	Vehicle longitudinal velocity

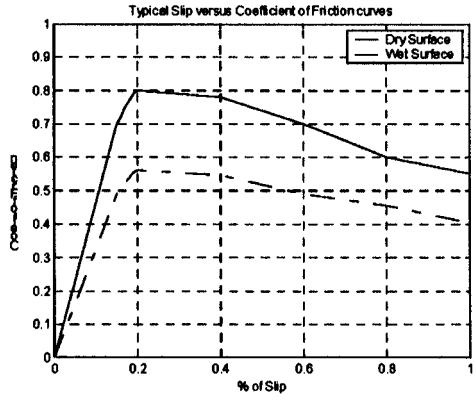

FIGURE 8.1 Slip versus coefficient of friction curves for surfaces.

is not available. Assume that $f(\lambda)$ is the function to be maximized and this function has only one extreme point. The design of sliding mode self-optimization system is performed based on [14, 15]. The basic idea of the theory is to design sliding mode control to force the system to track an introduced monotonously increasing function $\dot{g}(t) = \rho_0$ where ρ_0 is positive constant.

Let the system output y be the tire tractive force F_{ti}. The forces may be measured directly by on-board accelerometer or it may be estimated by angular speed of wheels. Define the tracking error as $\varepsilon = g - y$ and let $s_1 = \varepsilon$ and $s_2 = \varepsilon + \delta$ where δ is the design parameter to be selected and g is a monotonously increasing function described by $\dot{g} = \rho_0$, $\rho_0 > 0$. Note that the braking torque, T_{b1}, is handled as a control action which may have two different values, $(-F_{t1}R_w)$ or $(T_{b1} - F_{t1}R_w)$. Then the motion equation w.r.t. angular velocity of one wheel, for example, the first one associated with the control algorithm, is of the form

$$J_w\dot{\omega}_1 = -B_t\omega_1 - u$$

where u is the control input from sliding mode optimizer,

$$u = \begin{cases} T_{b1} - F_{t1}R_w & s_1 s_2 > 0 \\ -F_{t1}R_w & s_1 s_2 < 0 \end{cases}$$

Modify reference function $g(t)$ by adding a double-hystereses component (as shown in Fig. 8.2)

$$\dot{g} = \rho_0 + Mv(s_1, s_2).$$

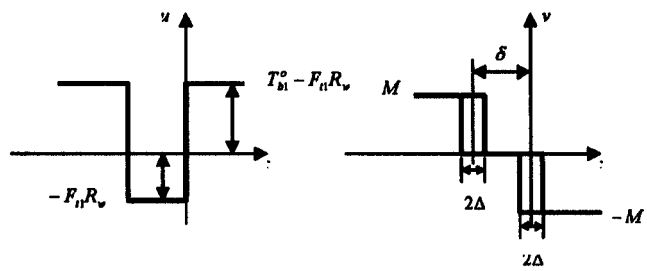

FIGURE 8.2 Control input $u(s_1 s_2)$ and double-hystereses function $Mv(s_1, s_2)$.

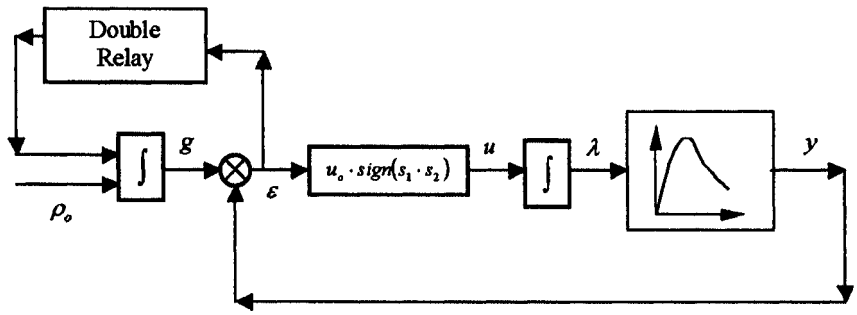

FIGURE 8.3 Sliding mode self-optimizer.

By enforcing sliding mode on either the surface $s_1 = 0$ or $s_2 = 0$, the system output can be maximized by tracking the reference function $g(t)$, As for the rest of the wheels, their control signals follow the first wheel (or the master wheel) where the proposed sliding mode optimizer is installed. Schematic diagram of self-optimizer is shown in the following Figure 8.3 which reveals the whole control design.

The following simulation is performed under the scenario that no on-board accelerometer is available and, initially, constant brake torque is applied at the very first beginning to totally lock up all wheels. Common drivers usually apply full brake under urgent situation. This status is compliant with the first moment when maximum vehicle deceleration is demanded. The controllers take over after 0.2 second to regulate brake torque. As can be seen from the following Figure 8.4, controllers are capable of reaching optimal slip after 0.5 second and the optimal level is maintained during whole braking process.

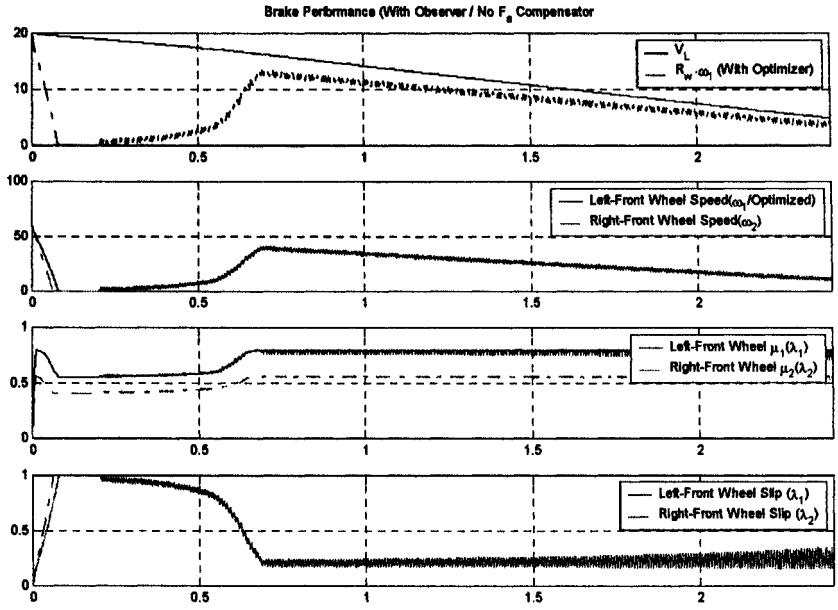

FIGURE 8.4 Braking performance after wheels are locked up.

References

[1] Mohan, N., Undeland, T. M. and Robbins, W. P. (1995) *Power Electronics*, John Wiley and Sons.

[2] Utkin, V., Chen, D. S., Zarei, S. and Miller, J. (2000) Nonlinear estimator design for automotive alternator utilizing battery current and speed measurements, *European Journal of Control*, **6**(2), 135–149.

[3] Utkin, V. (1991) *Sliding Models in Control and Optimization.* Berlin: Springer Verlag.

[4] Utkin, V., Guldner, J. and Shi, J. (1999) *Sliding Mode Control in Electrochemical Systems*, Taylor & Francis.

[5] Turin, R. C. and Geering, H. P. (1994) Model based adaptive fuel control in an SI engine, SAE Technical Paper, NO. 940374, 1994.

[6] Kim, Y. W., Rizzoni, G. and Utkin, V. (1998) Automotive engine diagnosis and control via nonlinear estimation, *IEEE Control Systems*, **18**(5), 84–99.

[7] Kim, Y. W., Rizzoni, G., Soliman, A., Azzoni, P. and Moro, D. (1997) Powertrain diagnostic using nonlinear sliding mode observer, *Proceedings of the IFAC/IMACS Sysmposium SAFEPROCESS'97.* UK: Hull, pp. 825–830.

[8] Didoruk, A., Yan, Z., Guven, M. and Utkin, V. (2001) A sliding mode speed and rotor time constant observer for induction machines, *Proceedings of International IEEE Conference, IECON'01*, Denver, Colorado, Nov. 29–Dec. 2, 2001, pp. 1400–1405.

[9] Krishnaswami, V. (1996) Model based fault detection and isolation in nonlinear systems, *Ph. D. Dissertation*, The Ohio State University.

[10] Jankovic, M., Jankovic, M. and Kolmanovsky, I. (1998) Robust nonlinear controller for turbocharged diesel engines, *Proceedings of the American Control Conference*, pp. 1389–1394.

[11] Luk'yanov, A. and Utkin, V. (1981) Methods of reducing dynamic systems to a regular form, *Automation and Remote Control*, (1), 5–13.

[12] Utkin, V. I., Chang, H.-C., Kolmanovsky, I. and Cook, J. (2000) Sliding mode control for variable geometry turbocharged diesel engine, *ACC2000*, Chicago, pp. 584–588.

[13] Korovin, S. and Utkin, V. (1972) Use of the slip mode in problems of static optimization, *Automation and Remote Control*, **33**(4) (p. I), 570–579 (in Russian).

[14] Korovin, S. and Utkin, V. (1974) Using sliding modes in static optimization and nonlinear programming, *Automatica, Journal of IFAC*, 10.

[15] Utkin, V. (1974) *Sliding Modes and Their Applications in Variable Structure Systems.* Moscow: Nauka (in Russian, English translation by MIR, 1978).

[16] Utkin, V. I., Chang, H.-C. and Keyhani, A. (2002) Sliding mode control for automobile air conditioner, *IFAC 2002*, Barcelona, Spain.

[17] Drakunov, S. and Utkin, V. I. (1995) Discrete event sliding mode observers for continuous time systems, *Proceedings of the 34th Conference of Decision and Control*, New Orleans, LA.